Insights into characteristics and formation mechanisms of secondary organic aerosols in Guangzhou urban area

Miaomiao Zhai[1,3], Ye Kuang[1,3*], Li Liu[2,*], Yao He[1,3], Biao Luo[1,3], Wanyun Xu[4], Jiangchuan Tao[1,3], Yu Zou[2], Fei Li[2,5], Changqin Yin[2,7], Chunhui Li[2], Hanbing Xu[6], Xuejiao Deng[2]

[1] Institute for Environmental and Climate Research, Jinan University, Guangzhou, China.

[2] Key Laboratory of Regional Numerical Weather Prediction, Institute of Tropical and Marine Meteorology, China Meteorological Administration, Guangzhou, 510640，China

[3] Guangdong-Hongkong-Macau Joint Laboratory of Collaborative Innovation for Environmental Quality, Guangzhou, China.

[4] State Key Laboratory of Severe Weather & Key Laboratory for Atmospheric Chemistry, Institute of Atmospheric Composition, Chinese Academy of Meteorological Sciences, Beijing, 100081, China

[5] Xiamen Key Laboratory of Straits Meteorology, Xiamen Meteorological Bureau, Xiamen, 361012, China

[6] Experimental Teaching Center, Sun Yat-Sen University, Guangzhou 510275, China

[7] Shanghai Key Laboratory of Meteorology and Health, Shanghai Meteorological Bureau, Shanghai 200030, China

*Correspondence to: Ye Kuang (kuangye@jnu.edu.cn) and Li Liu (liul@gd121.cn)

Abstract

Emission controls have substantially brought down aerosol pollution in China, however, aerosol mass reductions have slowed down in recent years in the Pearl River Delta (PRD) region, where secondary organic aerosol (SOA) formation poses a major challenge for air quality improvement. In this study, we characterized the roles of SOA in haze formation in urban Guangzhou City of the PRD using year-long aerosol mass spectrometer measurements for the first time and discussed possible pathways of SOA formations. On average, organic aerosols (OA) contribute dominantly (50%) to non-refractory submicron aerosol mass (NR-PM_1). The average mass concentration of SOA (including by less and more oxidized OA, LOOA and MOOA) contributed most to NR-PM_1, reached about 1.7 times that of primary organic aerosols (POA, including hydrocarbon-like and cooking-related OA) and accounting for 32% of NR-PM_1, even more than sulfate (22%) and nitrate (16%). Seasonal variations of NR-PM_1 revealed that haze formation mechanisms differed much among distinct seasons. Sulfate mattered more than nitrate in fall, while nitrate was more important than sulfate in spring and winter, with SOA contributing significantly to haze formations in all seasons. Daytime SOA formation was weak in winter under low oxidant level and air relative humidity, whereas prominent daytime SOA formation was observed in fall, spring and summer almost on daily basis, suggesting for important roles of photochemistry in SOA formations. Further analysis showed that the coordination of gas-phase photochemistry and subsequent aqueous-phase reactions likely played significant roles in quick daytime SOA formations. Obvious nighttime SOA formations were also frequently observed in spring, fall and winter, and it was found that daytime and nighttime SOA formations together had resulted in the highest SOA concentrations in these seasons and contributed substantially to severe haze formations. Simultaneous increases of nitrate with SOA after sunset suggested the important roles of NO_3 radical chemistry in nighttime SOA formations, and confirmed by continuous increase of NO^+/NO_2^+ fragment ratio that related to measured particulate nitrate after sunset. Findings of this study have promoted our understanding in haze pollution characteristics of the PRD and laid down future directions on investigations of SOA formation mechanisms in urban areas of southern China that share similar emission sources and meteorological conditions.

1 Introduction

Ubiquitous submicron aerosols in the atmosphere not only deteriorate human health and visibility, but also impact climate through interactions with solar radiation and clouds. Organic aerosols (OA) represent one of the most important and sometimes even dominant components (~10-90%) of PM_1 (aerosol particles with aerodynamic diameter less than 1 μm) in urban, rural and remote areas (Zhang et al., 2007;Jimenez et al., 2009). OA can either be emitted directly from emission sources or be formed through atmospheric reactions of volatile organic compounds, the former is referred to as primary OA (POA) and the latter is referred to as secondary OA (SOA). An increasing number of researches show that SOA account for a large fraction of OA worldwide (Zhang et al., 2007;Zhang et al., 2011), and even dominate in some cases (Kuang et al., 2020). The implementation of strict emission reduction policies has significantly improved the air quality of Pearl River Delta (PRD) region, which is a highly industrialized area of China, and the annual mean concentration of $PM_{2.5}$ (particulate matter with aerodynamic diameter less than 2.5 μm) has been brought down to less than 30 $\mu g/m^3$ (Xu et al., 2020). However, the reduction of $PM_{2.5}$ mass concentrations in PRD has slowed down substantially in recent years, which might be related to the significant increases in the proportion of secondary aerosols (Xu et al., 2020), especially for SOA. Insights into SOA formation mechanisms are important for air pollution improvement.

SOA formation mechanisms are a scientific hotspot of atmospheric chemistry in recent ten years since significant contributions of SOA to atmospheric aerosol mass were fully recognized (Zhang et al., 2007;Jimenez et al., 2009), however quite complex due to varying precursors, oxidants and formation pathways under different emission characteristics and meteorological conditions. As to SOA formation pathways, SOA can be formed through condensation of oxidized gas-phase organic vapors during the oxidation of volatile organic compounds (VOCs), this type of formed SOA was usually referred to as gasSOA (Kuang et al., 2020). SOA can also be formed in the aqueous phase through the further oxidation of dissolved VOCs which are usually products of gas-phase oxidation of VOCs, this type of SOA was usually referred as aqSOA (Ervens et al., 2011). Both field measurements and laboratory studies are needed in investigating detailed SOA formation mechanisms in different regions with field measurements provide insights into key oxidants and formation pathways, thus information from field measurements are important for both designing laboratory experiments and targeting

emission control strategies. Aerosol mass spectrometers are advanced on-line instruments that provide real time quantitative characterization of aerosol particle compositions (Jayne et al., 2000;Canagaratna et al., 2007;Jimenez et al., 2003). Positive matrix factorization (PMF) (Ulbrich et al., 2009) or a multilinear engine (ME-2) (Paatero, 1999;Canonaco et al., 2013) can be employed to further resolve different OA factors that are associated with different sources and formation mechanisms from the OA mass spectra. Using this technique, the SOA sources and formation mechanisms are extensively investigated in China (Zhou et al., 2020), and found that aqueous reactions in aerosol water contributed substantially even dominantly to SOA formations (Su et al., 2020) in haze episodes with daytime and nighttime SOA formations differ much due to different meteorological conditions and oxidants (Rollins et al., 2012;Huang et al., 2021).

In fact, in a specific region, the compositions, sources, and evolution processes differ much among seasons due to changes in emission sources and meteorological conditions (Li et al., 2015). Therefore, long-term observations that cover measurements of different seasons were usually needed for characterizing OA sources and SOA formation mechanisms, thereby helping to address the challenge of fine particulate matter pollution mitigation. Even though aerosol mass spectrometers have been widely used in China in recent years and the importance of long-term measurements, most studies have been conducted in specific periods due to its high cost and maintenance (He et al., 2011;Chen et al., 2021b;Qin et al., 2017), resulting in few long-term characterizations of the mass concentrations and chemical compositions of submicron particulate matter (PM_1). The design of Aerosol Chemical Speciation Monitor (ACSM) has improved this problem to some extent (Ng et al., 2011;Sun et al., 2015;Canonaco et al., 2021). For example, based on 2-year ACSM measurements, Sun et al. (2018) investigate the distinct characteristics of PM_1 compositions among different seasons in Beijing urban area and illustrated the dominant role of SOA in OA across different mass loading scenarios during all seasons.

Guangzhou is an expansive metropolis in the highly industrialized PRD region. Using the aerosol mass spectrometer measurements and source apportionment technique, Qin et al. (2017) and Huang et al. (2011) reported that SOA contributed substantially to aerosol mass during autumn and winter in Guangzhou. Guo et al. (2020) found that OA played a dominant role in PM_1 during winter in Guangzhou, with OA source apportionment emphasized the dominance of SOA. Guo et al. (2020) also

suggested that gasSOA contributed predominantly to SOA formation during non-pollution periods, other mechanisms such as heterogeneous and multiphase reactions played more important roles in SOA formation during pollution episodes, however long-term aerosol spectrometer measurements hat help for characterizing OA source and SOA formation mechanisms in this region remain lacking. In this study, we performed a year-long continuous measurement of non-refractory submicron aerosols ($NR\text{-}PM_1$) with an ACSM in urban Guangzhou from September 2020 to August 2021 to characterize POA sources and investigate SOA formation mechanisms in different seasons.

2 Experimental methods

2.1 sampling site and measurements

A quadrupole-Aerosol Chemical Speciation Monitor (Q-ACSM) was deployed to continuously measure nonrefractory PM_1 ($NR\text{-}PM_1$) species including OA, sulfate (SO_4), nitrate (NO_3), ammonium (NH_4), and chloride (Cl) from September 2020 to August 2021 at an urban site located in Haizhu wetland park of Guangzhou, which is surrounded by commercial streets and residential buildings, however, with a distance of at least 1 km (Liu et al., 2022). Therefore, measurements at this site are representative of the pollution characteristics of Guangzhou urban area. More detailed descriptions about the sampling site and the ACSM measurements could be referred to Liu et al. (2022) and Ng et al. (2011), respectively. An AE33 aethalometer (Drinovec et al., 2015) set up with a flow rate of 5 L/min was separately operated downstream of a $PM_{2.5}$ inlet (BGI SCC 1.829) to measure aerosol absorptions, from which optically equivalent black carbon (BC) mass concentrations in winter and early spring were calculated. In addition, mass concentrations of $PM_{2.5}$ and trace gases such as nitrogen dioxide (NO_2), ozone (O_3), carbon monoxide (CO) and sulfur dioxide (SO_2) were acquired from the publicly available datasets of the China National Environmental Monitoring network (http://www.cnemc.cn/en/), which includes a site located within 5 km distance to our observation site. Measurements of meteorological parameters such as temperature, wind speed and direction (WS and WD), and relative humidity (RH) were made by an automatic weather station (Li et al., 2021). Aerosol liquid water content (ALWC) was predicted with the ISORROPIA-II thermodynamic model in reverse mode under metastable assumption (Guo et al., 2017) with aerosol chemical compositions measured

by Q-ACSM as inputs, with more details in Supplement Sect.S2.

2.2 Q-ACSM data analysis

The Q-ACSM data were processed using ACSM standard data analysis software (ACSM Local 1.5.10.0 Released July 6, 2015) written in Igor Pro (version 6.37). The composition-dependent collection efficiency (CE) parameterization scheme proposed by Middlebrook et al. (2012) was chosen to determine the mass concentrations of NR-PM_1 species which was also detailed in Liu et al. (2022). Relative ionization efficiencies (RIEs) of 5.15 and 0.7 were adopted for ammonium and sulfate quantifications which were calibrated using 300 nm pure NH_4NO_3 and $(NH_4)_2SO_4$ while the default RIEs of 1.4, 1.1 and 1.3 was used for organic aerosol, nitrate and chloride, respectively. Moreover, we also compared the mass concentrations of NR-PM_1 with $PM_{2.5}$ to ensure the validity of ACSM data during the whole study. As shown in Fig. S1 of the supplement, the measured NR-PM_1 correlates highly with $PM_{2.5}$ acquired from the nearest (about 5 km) Environmental Protection Agency site (R^2 = 0.71), and the average ratio of NR-PM_1/$PM_{2.5}$ is 0.77 (±0.36).

Unconstrained Positive matrix factorization (PMF) was performed on OA mass spectra of the entire year-long dataset. For the two-factor solution, the POA factor peaked in the evening with low O/C (~0.28) and an oxygenated OA (OOA) factor peaks in the afternoon with high O/C (~0.88) can be well resolved (Fig.S2), demonstrating the markedly different influences of primary emissions and SOA formations on diel aerosol mass concentrations. However, PMF-ACSM analysis of mass spectra of OA measured by unit mass resolution instruments still faced some uncertainties to further resolve potential POA or SOA components due to its rotational indeterminacy. For example, traffic-related hydron-carbon like organic aerosols (HOA) was uneasily to separate from cooking-related organic aerosols (COA) and there was also great uncertainty in distinguishing SOA with different degrees of oxidations (Sun et al., 2012;Sun et al., 2013;Zhang et al., 2015). Therefore, an improved source apportionment technique called Multilinear Engine (ME-2) was further used to resolve better sources of POA and SOA (Paatero, 1999;Canonaco et al., 2013;Guo et al., 2020). Previously, both Guo et al. (2020) and Liu et al. (2022) demonstrated that during both autumn and winter seasons of Guangzhou urban areas, POA was mainly composed of HOA, which is mostly associated with traffic emissions and COA, and SOA could be resolved into less oxidized and more oxidized organic aerosols (LOOA

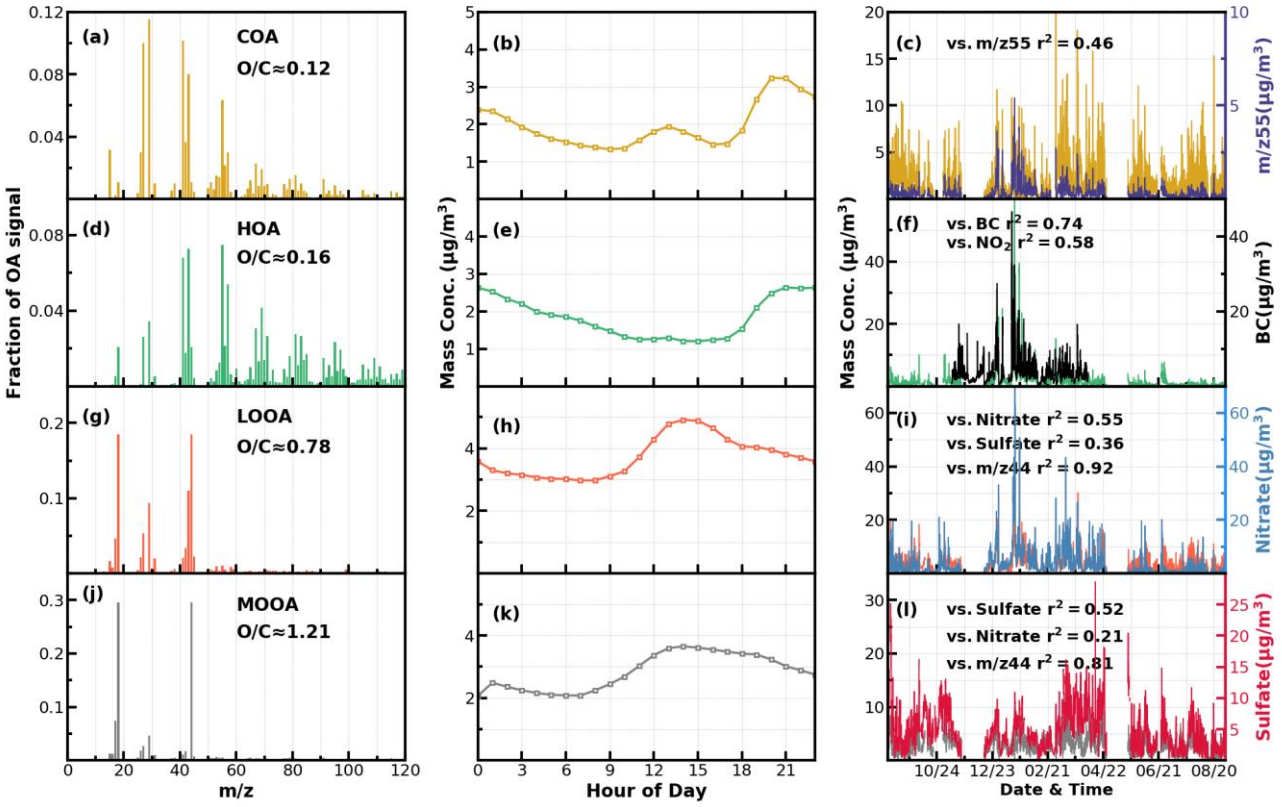

Figure 1. Mass spectral profiles, diurnal cycles and correlations with external data of COA**(a-c)**, HOA**(d-f)**, LOOA**(g-i)** and MOOA**(j-l)** from ME2-ACSM analysis for the entire year.

and MOOA). The number selecting test using unconstrained PMF analysis (Fig.S3) also showed that four-factor solution likely be the best choice. Therefore, we had chosen 4 factors for ME-2 analysis with the *a* value of ME-2 ranges from 0.1 to 0.5, and constrained the HOA and COA profiles with HOA and COA profiles reported in Liu et al. (2022) as priories considering the following three reasons: (1) The used instrument of this study is the same one of Liu et al. (2022); (2) the COA profile reported in Liu et al. (2022) was determined during the period when both COVID-19 silence-action and festival spring occurred when cooking activities grew and traffic activities almost vanished thus COA shall dominated over HOA, more details about the method please refer to Liu et al. (2022); (3) Resolved variations of HOA and COA are well explained by external datasets such as correlations of HOA with black carbon reached 0.79. The four-factor solution using the ME-2 technique with a=0.2 was obtained and shown in Fig.1. The resolved HOA and COA are summed as POA, resolved LOOA and MOOA are summed as SOA, and the comparison with those resolved by the PMF is shown in Fig.2. ME-2 analysis generally reproduced both the diurnal variations as well as absolute mass concentrations of POA and SOA during different months well. To explore the consistency of resolved factors using the

entire year-long dataset or only using seasonal dataset when performing ME-2 analysis, we performed individual ME-2 runs for each season. Results showed that factors resolved in each season using seasonal datasets as inputs of ME-2 are generally consistent with those resolved from year-long dataset (Fig.S4-S7). Therefore, factors resolved using the entire year-long dataset as input of ME-2 were used for further investigations and this also guaranteed consistency of factors for comparisons among seasons.

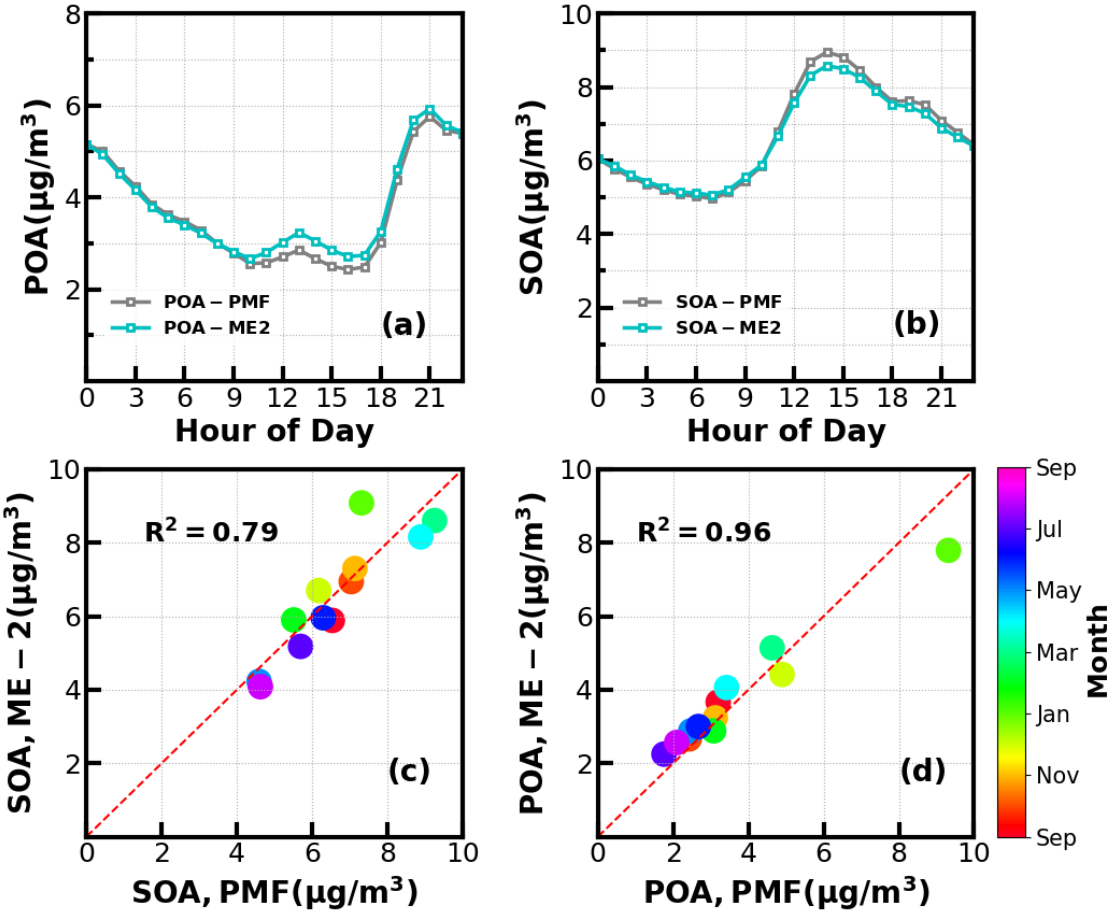

Figure 2. (a) and **(b)** Diurnal variations of POA and SOA concentrations from ME-2 and PMF; **(c)** and **(d)** Scatter plots between monthly average POA and SOA concentrations from ME-2 and PMF.

The mass spectrum of COA deconvolved in this work was characterized by a high m/z 55-to-57 ratio of 2.12, which was the same with the one reported by Guo et al. (2020), and close to the m/z 55-to-57 ratio range of 2.2-2.8 reported by Mohr et al. (2012) for COA. Similar to previous studies (Guo et al., 2020;Sun et al., 2013), the concentration of COA was well correlated (R^2=0.46) with m/z 55. The O/C ratio of 0.12 for COA revealed that it was less oxidized than HOA (O/C=0.16) during the whole year in Guangzhou, which was contrary to Sun et al. (2011). As shown in Fig.3, the diurnal profile of COA presented two typical peaks during the entire year with a noontime peak during 13:00

- 14:00 LT and an evening peak during 20:00 - 21:00 LT, which were associated with noon and evening cooking activities. It was noteworthy that the nighttime peak concentration of COA was very close to that of noontime in summer, while the evening peak of COA was significantly higher than that of noontime in other three seasons. The ratio of evening COA peak to that of the noontime was 1.7 in fall, and was 1.6 in spring. In particular, the evening COA peak was nearly 4 times that of noontime in winter due to the relatively insignificant noontime peak during this period, which might be associated

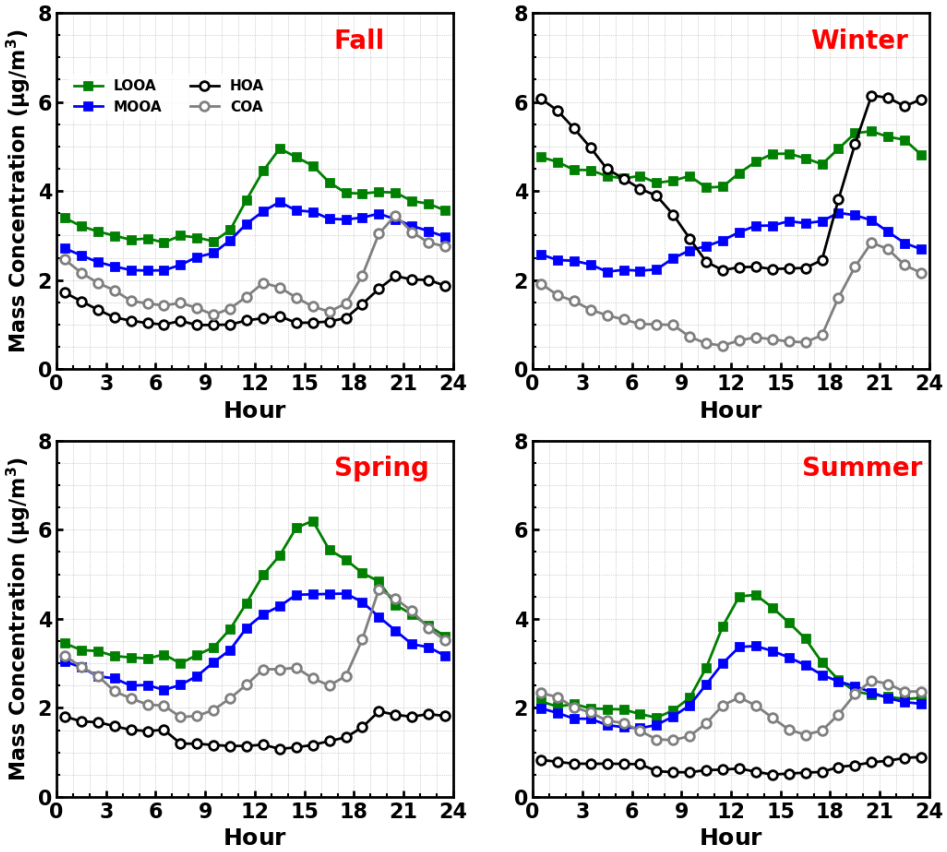

Figure 3. Diurnal profiles of HOA, COA, LOOA and MOOA in spring (March to May), summer (Jnue to August), Fall (September to November), Winter (December to February).

with the lock down and spring festival in winter which resulted in less noontime activities. Similar conclusions could be found in Sun et al. (2018). More frequent cooking activities at night such as the Chinese habit of eating midnight snacks, shallower boundary layer that inhibited diffusion of pollutants, and the lower temperature at night which facilitated semi-volatile compounds from cooking emissions to partition into particles resulted in the higher peak concentration at nighttime than at noon (Guo et al., 2020).

The mass spectrum of HOA (Fig.1b) was characterized with the $C_nH_{2n-1}^+$ (m/z = 27, 41, 55, 69) and $C_nH_{2n+1}^+$ (m/z = 29, 43, 57, 71) ion species. The concentration of HOA had a good correlation

with that of primary BC emission (R^2=0.74), and also correlated well with that of NO_2 (R^2=0.58), indicating considerable impacts of traffic emissions on the HOA mass loading. As shown in Fig.3, except for summer, HOA increased significantly after sunrise especially in winter, however, began to decrease in the late evening. HOA was significantly higher during nighttime than during daytime in all seasons especially in winter, however, was not obvious in summer. HOA mass concentration peaks around 20:00 LT were attributed to traffic emissions during the nocturnal rush hours. However, the continuously high concentrations of HOA after 20:00 until 02:00 of the next day might have resulted from heavy-duty vehicles with daytime traffic restrictions in Guangzhou (Guo et al., 2020;Qin et al., 2017).

Two OOA factors were characterized with high O/C ratio, LOOA with O/C of 0.78 and MOOA with O/C of 1.2, suggesting high oxidation degrees of SOA factors in Guangzhou urban area, especially that of MOOA. MOOA and LOOA shared similar diurnal profiles regardless of seasons, with MOOA showed higher correlations with sulfate and LOOA showed higher correlations with nitrate. MOOA and LOOA increased together in fall from 09:00 LT until 14:00 LT reached a maximum of 3.7 μg/m^3 for MOOA and 5 μg/m^3 for LOOA, followed by a gradual decrease in SOA concentrations and then remained relatively flat. The diurnal profiles of SOA in spring and summer were relatively similar to those in fall, however, more remarkable decreases of SOA from afternoon to midnight were observed in spring and summer. This is because SOA sometimes increased after sunset in autumn, which was even more prominent in winter, where LOOA and MOOA would first increase for a while after sunset and then begun to decrease. However, weaker daytime SOA formation was observed in winter. Note that a aqSOA factor (called aqOOA in these references) was previously resolved using the aerosol mass spectrometer measurements (Sun et al., 2016;Zhao et al., 2019) or time-of flight ACSM measurements (Lei et al., 2021), and the factor was resolved as aqSOA because of its high fraction of m/z 29 (CHO+) and high correlation with sulfate. Both two resolved SOA factors in this study showed relatively weak correlations with sulfate (Fig.1), do not support directly if they are related with aqueous phase reactions.

3 Results and discussion

3.1 The largest contribution of secondary organic aerosols in NR-PM_1

Time series of the meteorological parameters (including RH, WS and WD), the mass concentrations of NR-PM_1 and $PM_{2.5}$, chemical compositions of NR-PM_1, trace gases and four resolved OA factors are shown Fig.S8. It shows that emission source intensities and meteorological variables changed dramatically among seasons. Hourly NR-PM_1 mass concentrations ranged from near zero to 177 μg/m^3 with an average of 21 μg/m^3. From October to February, northerly winds prevailed and average NR-PM_1 was relatively higher than that from February to September (26 vs 19 μg/m^3), which were associated with relatively lower boundary height during cold seasons and northern winds brought polluted continental air mass. While during warm seasons of Guangzhou (March to September), south-easterly wind prevailed, which brought cleaner air mass from the ocean and the boundary layer height was higher due to more surface heating. Monthly variations of $PM_{2.5}$ are shown in Fig.4a, $PM_{2.5}$ in summer was lowest and around 16 μg/m^3 from May to August which were likely associated with the prevalence of rainy conditions in summer (Fig.S9) and possible higher boundary layer height (Yang et al., 2013). January was the month with highest $PM_{2.5}$ mass concentrations with an average of 49 μg/m^3, which was consistent with the fact that winter usually experienced the worst air pollutions due to the stagnant air conditions.

The average mass contributions of different components to NR-PM_1 during the entire year and among different seasons are shown in Fig.4b-4f. On average OA contributed about 50% to NR-PM_1 with the highest contribution in summer that reached near 57% and lowest contribution in spring of about 47%. The second largest contributor was sulfate, which on average contributed about 22%, and more than 20% in spring, summer and fall. However, the contribution of nitrate to NR-PM_1 (23%) exceeded that of sulfate (14%) and became the second major component after OA in winter, consistent with the results of Guo et al. (2020) for pollution periods in winter of Guangzhou. The probability distributions of mass concentrations of OA, sulfate and nitrate are shown in Fig.4g-4i. Both OA and nitrate were distributed in wide ranges during winter and shared similar shape of probability distribution, with OA increasing gradually from summer to winter and then reducing in the spring. Sulfate shared similar magnitudes in summer and winter, and differed much from those in spring and

fall that had higher sulfate concentrations and varied in a wider range. Nitrate in summer and fall were relatively lower in summer and fall, however, had much higher concentrations in spring and winter.

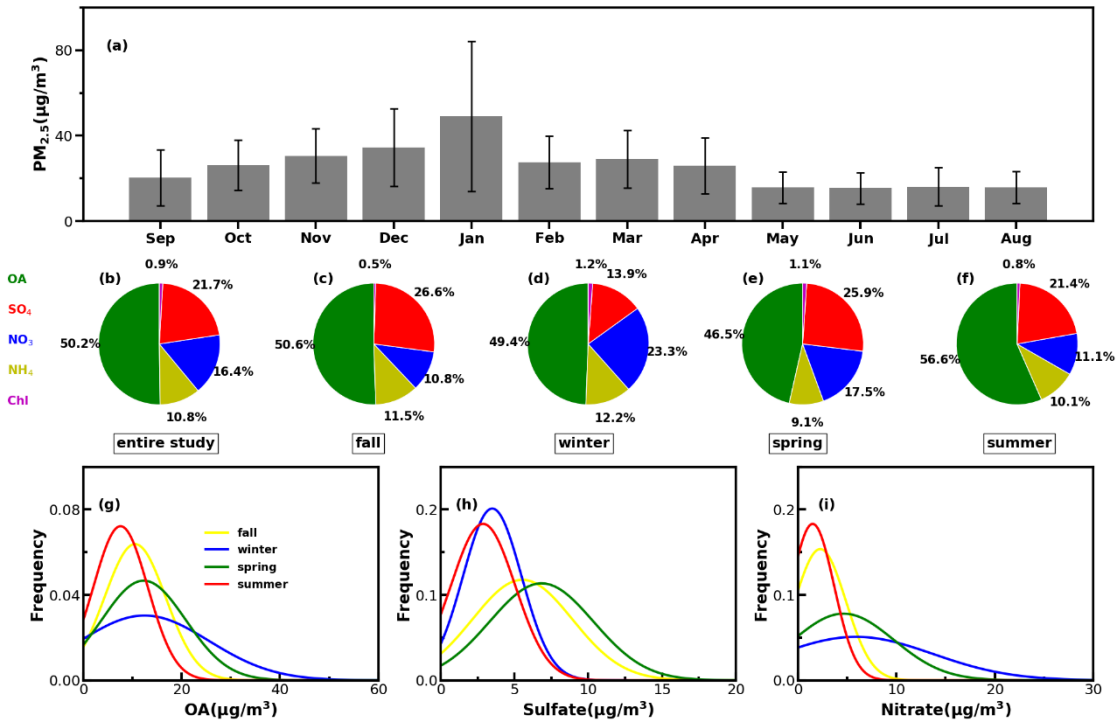

Figure 4. (a) Monthly average $PM_{2.5}$ mass concentrations from September of 2020 to August of 2021; **(b)-(f)** The average mass fractions of the chemical components in NR-PM_1 of the entire year and different seasons; **(g)-(i)** Probability distributions of OA, sulfate (SO_4) and nitrate (NO_3) in different seasons.

As shown in Fig.5a, average OA concentrations of different months ranged from about 7 μg/m^3 to 17 μg/m^3 with the peak in January and the lowest in August, and the variations of OA mass concentration in winter and spring were much larger than those in summer and autumn. Monthly variations of mass concentrations of the four resolved factors are shown in Fig.5b-5e, and contributions of the four OA factors to OA are shown in Fig.5f. In general, HOA remained lower than 2 μg/m^3 in most months, however, as the cold season approached from November, the monthly average OA increased substantially from about 2 μg/m^3 to near 6 μg/m^3. The much lower temperature and accumulation favorable meteorological conditions likely had resulted in the substantial increase of HOA. Compared with HOA, the seasonal variations of COA were less pronounced. The monthly average concentration of COA in warm months (February to October) was higher than those in cold months (October to January). The lowest monthly average concentration of COA was about 1 μg/m^3 which occurred in February when the contribution of COA to OA was near its lowest of about 9%. Overall, COA contributed about 19% of OA during the whole year which was close to that of HOA

(18%). However, the contributions of COA and HOA to total OA differ much among seasons. The contributions of COA to OA were higher than that of HOA during warm months and lower than that of HOA in relatively cold months especially in winter. These results highlight the significant contributions of POA to OA in Guangzhou urban area, however, contributions of emission sources differed much among cold and warm seasons.

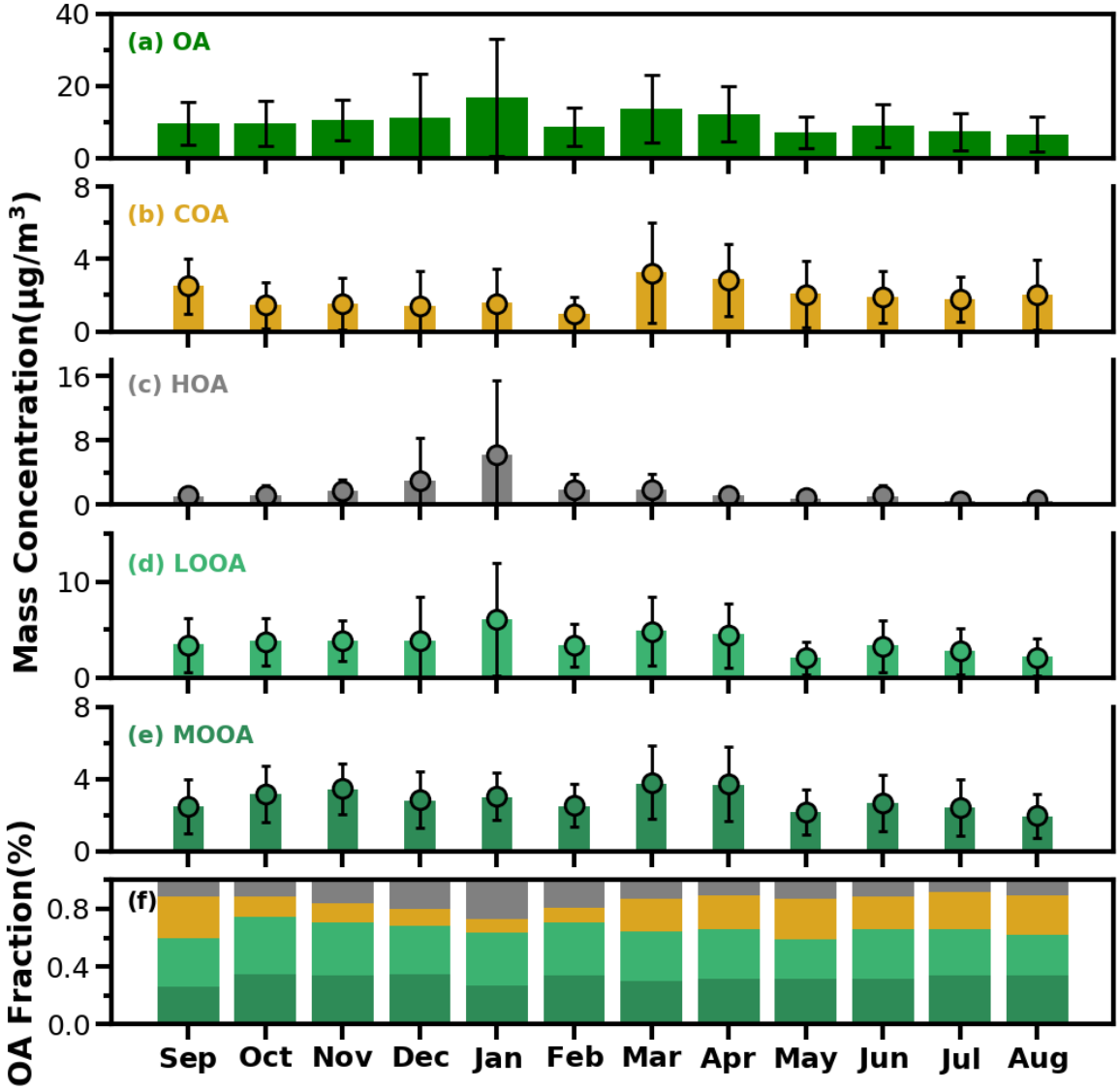

Figure 5. The bar plots of monthly average mass concentrations of OA, COA, HOA, LOOA and MOOA from **(a) to (e)** and mass fractions of OA factors in OA **(f)**.

SOA (MOOA+LOOA) contributed more than 60% to OA in all months, reached beyond 70% in October and February, and made up on average 63% of OA in the entire year. As shown in Fig.5(e-f), LOOA exhibited stronger seasonal variations than MOOA, with monthly average mass concentrations of LOOA varying between 2.6 to 6.1 μg/m^3 and monthly average MOOA concentration ranging from

2 to 3.8 μg/m^3. The LOOA mass concentration peaked in the most polluted month of January, suggesting that significant contributions of LOOA formation to severe haze pollution in winter. The contribution of LOOA to OA ranged from 27% to 39% with an average of 34%, and the contribution of MOOA to OA ranged from 26% to 35% with an average of 32%. Overall, the average mass concentration of SOA was about 1.7 times that of POA for the whole year, and SOA accounted for about 32% of NR-PM_1, which was higher than those of sulfate and nitrate, demonstrating the largest contribution of SOA to NR-PM_1.

3.2 Significant contributions of secondary organic aerosols to haze formations in all seasons

Investigations on contribution variations of aerosol compositions under different aerosol pollution levels are helpful for understanding mechanisms of haze formations, and results in four seasons are presented in Fig.6. The chemical composition of NR-PM_1 under different pollution levels differ much among seasons. In fall, as demonstrated by variations of mass concentrations of aerosol compositions under different pollution levels shown in Fig.6, pollution conditions in fall were dominantly controlled by secondary formations of sulfate and SOA, accumulation of primary aerosols and nitrate formation had relatively smaller impacts. With respect to mass fractions variations, contributions of aerosol components differed much among different pollution levels. The fraction of OA decreased rapidly from 67% to 50% when the mass concentration of NR-PM_1 gradually increased to 15 μg/m^3, while the contribution of sulfate increased substantially from 17% to 30%, and the contribution of nitrate remained relatively stable at about 10%. When NR-PM_1 further increased, OA contribution remained relatively flat for NR-PM_1 below about 50 μg/m^3. Accordingly, the contribution of SO_4^{2-} decreased to ~18%, and the contribution of nitrate substantially increased from ~10 % to 21%. After that, OA contribution decreased rapidly to about 40% and then remained stable for NR-PM_1 >50 μg/m^3. However, the contribution of sulfate began to increase, and the highest contribution could account for 30%, while the contribution of nitrate began to decline gradually to 12%. In addition, the SOA contributed dominantly to OA (>60%) for NR-PM_1 > 15 μg/m^3 and even reached near 70% for NR-PM_1 > 35 μg/m^3, suggesting the dominant role of SOA in OA accumulations in haze events during fall.

In winter, haze formations are mostly associated with POA accumulations, SOA and nitrate formations, with nitrate formation playing the most important role, since it is also accompanied by

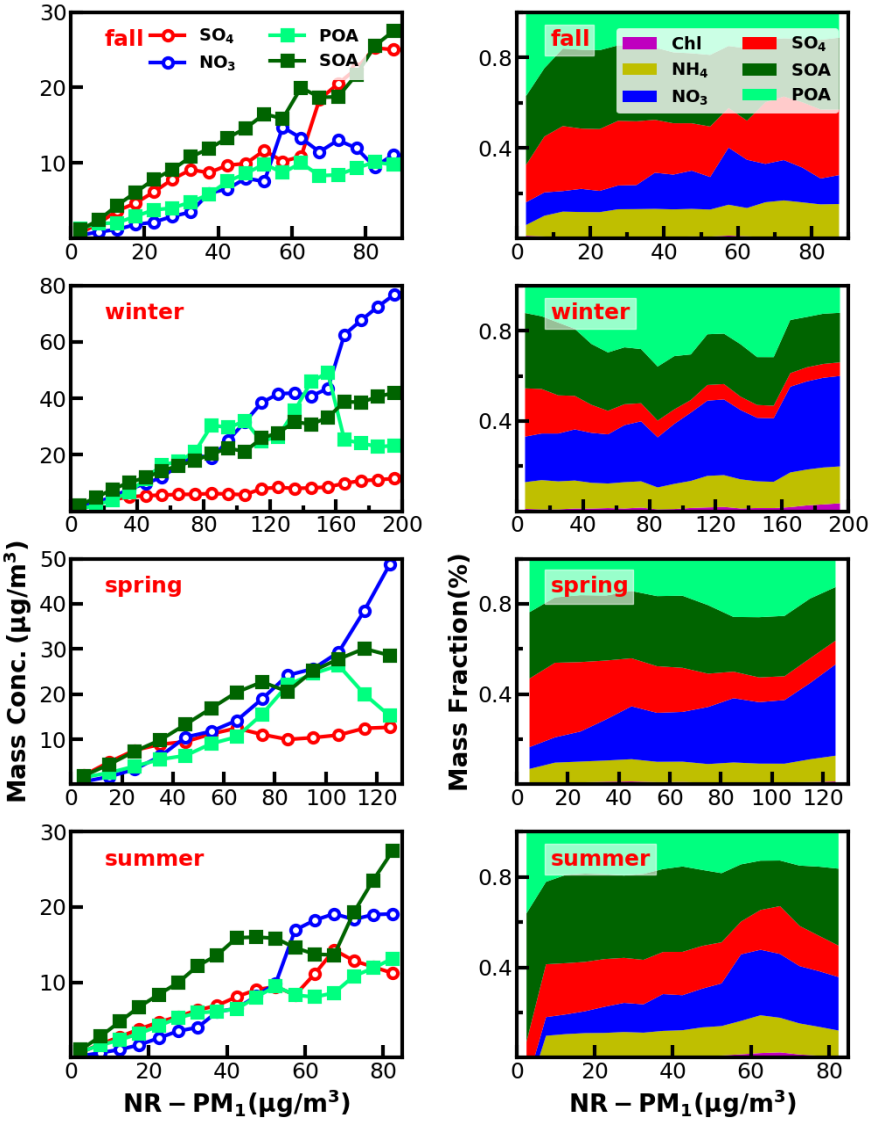

Figure 6. Left panels show absolute mass concentration variations of aerosol compositions under different NR-PM_1 levels, right panels show mass fractions of chemical components as a function of NR-PM_1.

ammonium formation, while sulfate formation was weak in winter. The fraction of OA increased gradually with the increase of NR-PM_1 concentration for NR-PM_1 < 90 μg/m^3 and reached the maximum of 60%, while the contribution of nitrate also showed a small increase from 21% to 26%. Under aggravating pollution, OA contribution fluctuated, however, showed a decreasing trend from 60% to ~40%. Meanwhile, the nitrate contribution showed an increasing trend from 26% to ~40%, which was similar to that of OA. Sulfate contribution decreased with the increase of NR-PM_1 concentration for NR-PM_1 < 100 μg/m^3 and then remained at about 6% as NR-PM_1 increases. In addition, the POA contribution increased about 25% to 50% for NR-PM_1 < 100 μg/m^3. Overall, the

increase of nitrate, POA and SOA together had resulted in severely polluted conditions in winter. The substantial contribution of POA to severe haze demonstrates that meteorological conditions unfavorable for the pollutant diffusion together with the substantial contributions of secondary nitrate and SOA formations have resulted in the most severe haze pollutions among the year. Especially, HOA contribution to OA increased from 17% to 52% when NR-PM_1 concentration was less than 140 μg/m^3, suggesting the significant role of traffic emission accumulation during severe haze pollution, which was consistent with results of Yao et al. (2020).

In spring, haze pollutions were mostly associated POA accumulation and secondary formations of nitrate and SOA, especially that of nitrate. The contribution of OA decreased from 51% to 44% as NR-PM_1 mass concentration increased when NR-PM_1 mass concentration was less than 50 μg/m^3. When the mass concentration of NR-PM_1 reached about 105 μg/m^3, the fraction of OA reached a maximum of 55%, and then decreased to about 37%. The most noticeable characteristic was the increase of nitrate contribution (from 10% to 40%) and decrease of sulfate contribution (32% to 10%) as the NR-PM_1 increased. In summer, secondary aerosol formations contributed dominantly to haze formations, with POA contribution to NR-PM_1 was about 20% in most conditions. The overall contribution of OA gradually decreased from near 60% to 35% as the mass concentration of NR-PM_1 increased for NR-PM_1 concentration < 60 μg/m^3 which was markedly different with those in other seasons, however increased to 49% as the NR-PM_1 concentration increased further. The contribution of sulfate decreased from 25% to 13% and the contribution of nitrate increased from 9.0% to 31% with the increase of NR-PM_1 concentration for NR-PM_1 concentration < 60 μg/m^3. While the OA was dominated by SOA under most conditions (about 60%).

Overall, haze formation mechanisms differed much among distinct seasons. Sulfate mattered more than nitrate in fall, while nitrate mattered more than sulfate in spring and winter, however, SOA contributed significantly to haze formations in all seasons. Note that seasonal variations of aerosol chemical compositions might differ much among years due to different meteorological conditions and emissions. For example, the evolution of sulfate during autumn in this study (Fig.S10) have remarkably different accumulation characteristics with those observed in autumn of 2018 as shown in Fig.1 of Chen et al. (2021a). Even so, SOA play significant roles in haze formations of Guangzhou urban area in all seasons hold based on results of existing literatures (Zhou et al., 2020).

3.3 Discussions on SOA formation mechanisms

As shown in Fig.3, both LOOA and MOOA mainly increased after sunrise, highlighting important roles of photochemistry in SOA formations. However, as demonstrated by Kuang et al. (2020), the daytime SOA formation could be either result from gas-phase photochemistry and subsequent condensation (gasSOA), or the result of gas-phase VOCs transformations with subsequent aqueous reactions (aqSOA). Especially since the PRD region is characterized by both active photochemistry due to strong solar radiation in subtropical regions and high relative humidity (annual average RH of ~75%), both photochemistry and aqueous phase reactions might play significant roles in SOA formation, however, this aspect was not explored before.

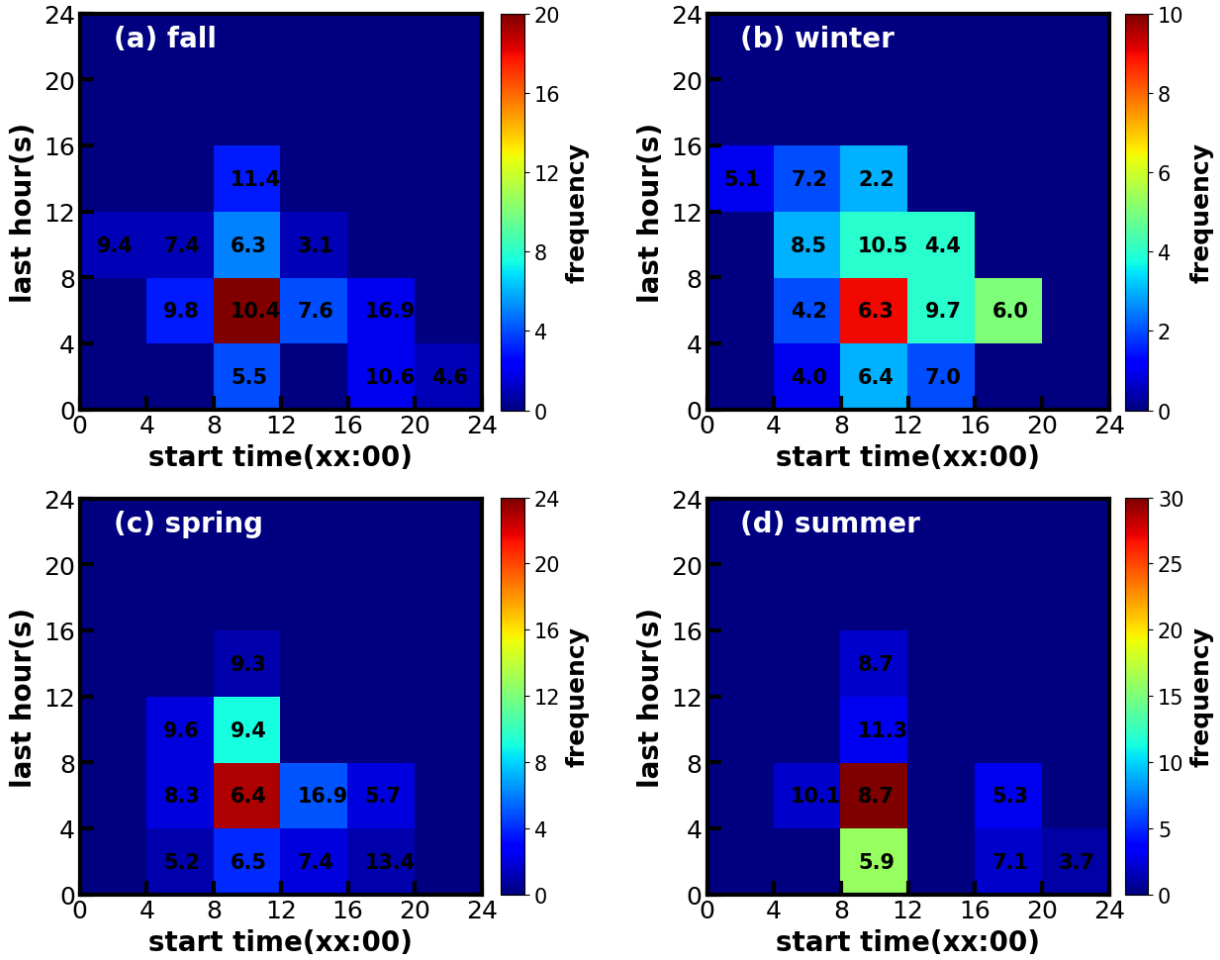

Figure 7. Time frequency diagrams of SOA increase events in **(a)** fall, **(b)** winter, **(c)** spring and **(d)** summer. X-axis represent start time of SOA increase, and y-axis represents the lasting hours of SOA increase events. The color scales indicate the number of occurrences. The values in the grid are the average SOA concentration during the SOA increase case.

Considering the frequent co-increase of MOOA and LOOA, they were grouped together as SOA for further investigations on their formation. SOA formation cases in four seasons were identified, the start time and lasting hours of their occurrences, as well as associated SOA levels are shown in Fig.7. Note that the identification of SOA formation cases has not considered the dilution effect of the lifting daytime boundary layer height and was only based on the absolute mass concentration variations. Therefore, this method has neglected some SOA formation cases that were masked by evolutions of the boundary layer, and the identified cases represent active SOA formation events that overcame dilution effects, which might be more suitable for further SOA formation investigations due to strong SOA formation signals. It shows that in all seasons, the SOA formation happened most frequently during daytime, starting in the morning and lasting about 4-8 hours. Especially, in spring, summer and fall, the daytime SOA formation almost happened everyday (Fig.S5-7), even if strong daytime boundary layer evolutions could be expected in these seasons due to strong surface solar heating, and resulted in the afternoon SOA mass concentration peaks in these seasons (Fig.3). However, highest SOA concentrations did not appear in the seasons with the most frequent morning to afternoon increases. Taking SOA formation cases in spring as an example, if the SOA increase started in the morning, more than 8 hours duration will result in significant higher SOA concentration. These cases started in the afternoon and lasted 4-8 hours would result in highest SOA concentration in spring. The SOA formation cases starting in the morning, however, only lasting within 4 hours, happened frequently in summer while less in spring and fall, suggesting that the absolute SOA mass concentration increase was more often stopped by strong boundary layer mixing in summer, which was consistent with the solar heating characteristics. The highest SOA in fall and winter were associated with the continuous increase of SOA after sunrise, suggesting that coordination of daytime and nighttime SOA formation together had resulted in the highest SOA concentrations in fall and winter.

To dig deeper into possible mechanisms behind the active daytime SOA formations throughout the year, we investigated relationships between SOA formation rates and both O_3 as well as aerosol liquid water content (ALWC) for the most frequent morning to afternoon SOA increase cases. Without considering the dilution effect of rising boundary layer, the daytime apparent growth rates of SOA varied from 0.2 to 4.4 $\mu g\ m^{-3}\ h^{-1}$ (Fig.8). Note that the SOA growth rates was calculated on the basis of observations of the first four hours for each SOA increase case to reduce impacts of boundary layer

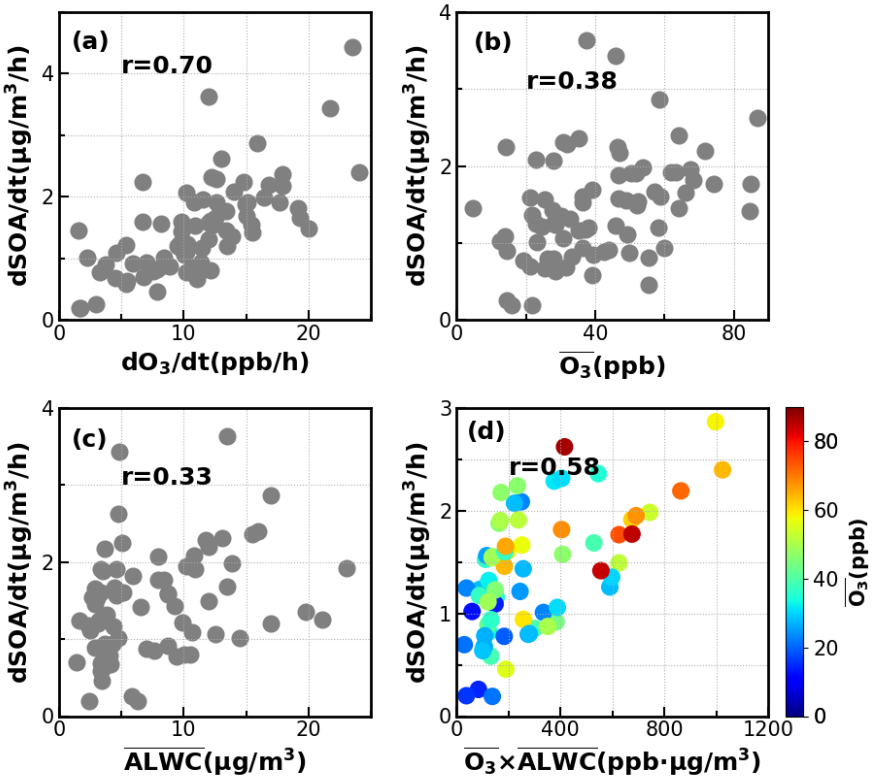

Figure 8. Relationships between SOA daytime formation rates with corresponding **(a)** O_3 formation rate; **(b)** average O_3; **(c)** average ALWC ($\mu g/m^3$) and **(d)** combination of averaged O_3 and averaged ALWC.

dilution effects. Some previous studies used variations of CO concentrations to partially correct for boundary layer dilution effects, however this method would fail in sites with strong CO emissions (Kuang et al., 2020). The SOA growth rates and were highly correlated to O_3 formation rates (r=0.7) as shown in Fig.8. However, this result only proved the important role of photochemistry in SOA formations. The apparent SOA growth rates showed positive but much weaker correlation with the average O_3 concentration during the period of SOA the increase (r=0.38), demonstrating that oxidant level was likely not the controlling factor for SOA formation, although O_3 alone did not represent the variations of oxidation levels and other sources such as HONO photolysis (Yu et al., 2022) also contribute to OH radicals and is a typical oxidant in daytime photochemistry. To investigate the possible roles of aqueous reactions in SOA formation, the relationship between apparent SOA rates and corresponding average ALWC were also investigated, and a positive but weak correlation was found (r=0.33). More importantly, the correlation coefficient between apparent SOA growth rates and the variable of average ALWC multiplying by average O_3 would be much higher (r=0.58, Fig.8d), suggesting that the coordination of gas-phase photochemistry and further aqueous reactions had likely

resulted in the rapid daytime SOA formations.

Besides the daytime SOA formation associated with photochemistry, dark transformations of VOCs that involve nighttime gas-phase and aqueous phase reactions might also result in efficient SOA formations. As shown in Fig.7, continuous increases of SOA were also frequently observed after sunset

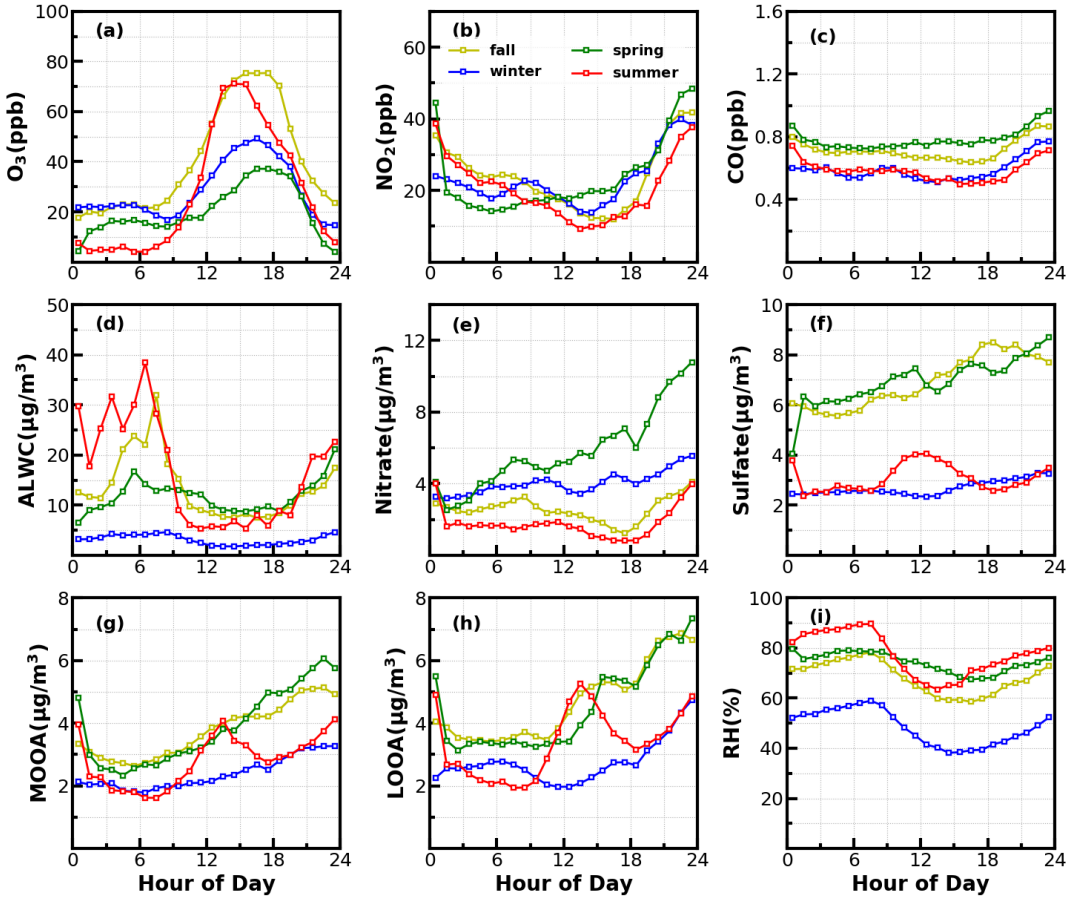

Figure 9. Average diurnal variations of **(a)** O_3; **(b)** NO_2; **(c)** CO; **(d)** ALWC; **(e)** nitrate; **(f)** sulfate; **(g)** MOOA; **(h)** LOOA and **(i)** RH for identified days with nighttime SOA increases.

in spring (17 days), fall (18 days) and winter (20 days) with sporadic occurrence in summer, and the coordination of daytime and nighttime SOA formations together have resulted in the highest SOA concentrations in fall and winter which were associated with severe haze pollutions as demonstrated above. Average diurnal profiles of O_3, NO_2, CO, RH, ALWC, nitrate, sulfate, LOOA and MOOA for cases with co-increases of LOOA and MOOA after 18:00 in different seasons are shown in Fig.9. On average, SOA usually showed decreases during nighttime (Fig.3) due to transport of air mass from cleaner suburban regions. The average wind speed was 1.7 m/s from 18:00 to 23:00 LT for identified nighttime SOA increase cases and was obviously lower than the corresponding average wind speed of

2.3 m/s, suggesting the more stagnant air mass tended to favor the nighttime SOA increases. However, the nighttime 5h back trajectories shown in Fig.S11 demonstrated that the nighttime replacement of surrounding suburban cleaner air mass still prevailed, therefore the continuous increases of SOA suggested that nighttime SOA formation occurred on a regional scale. The increases of LOOA and MOOA were accompanied with obvious nitrate formation in all seasons as well as slight increases of sulfate, further indicating for regional scale nighttime secondary aerosol formations during these nighttime SOA formation events. Except for summer, continuous increase of SOA from the morning to nighttime confirmed that the coordination of daytime and nighttime SOA formations had contributed to haze formations. Number of days for daily average NR-PM_1 ranges of 0-20, 20-35, 35-45, 45-60 and >60 $\mu g/m^3$ were 185,85,24,10 and 7, respectively (Fig.10a). All cases with daily average NR-PM_1 higher than 45 $\mu g/m^3$ occurred in fall, winter and spring. The corresponding average diurnal variations

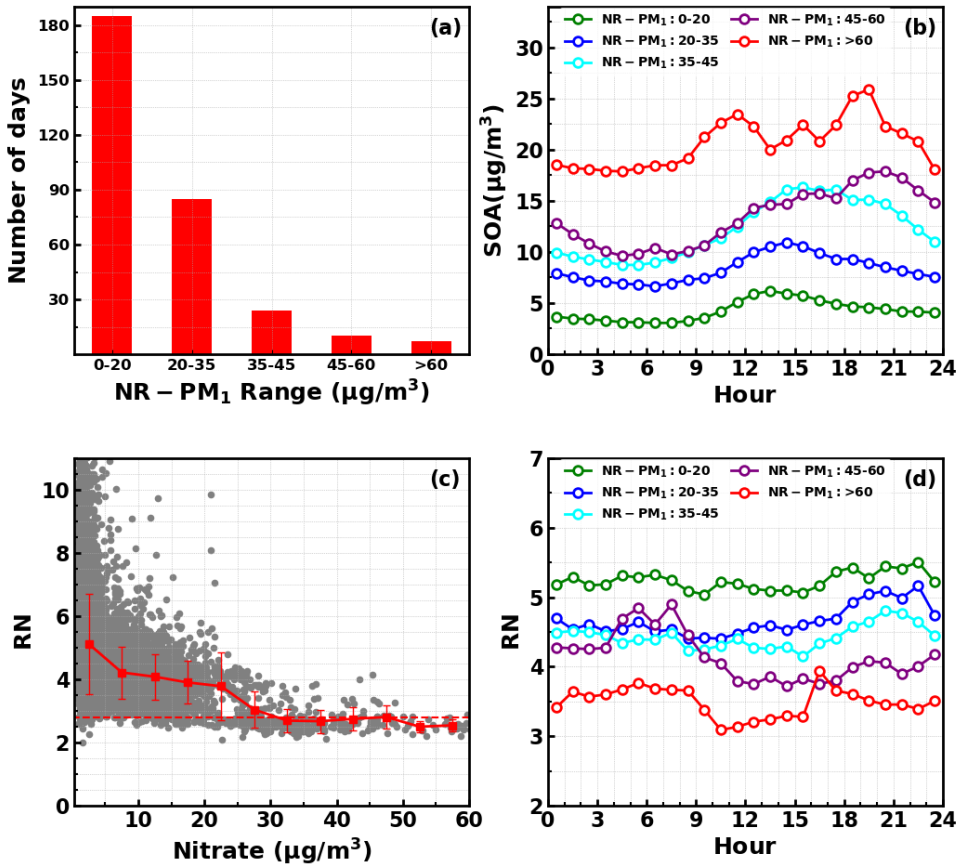

Figure 10. **(a)** Number of days in different daily average NR_PM_1 ranges; **(b)** Diurnal profiles of SOA under different NR_PM_1 ranges; **(c)** Variations NO^+/NO_2^+ (RN) as a function of measured nitrate, horizontal dashed line corresponds to RN of 2.8, red markers and bars represents averages and standard deviations; **(d)** Diurnal profiles of RN under different NR_PM_1 ranges.

of SOA for these relatively severe conditions shown in Fig.10b confirmed further that the coordination of daytime and nighttime SOA formations had contributed to severe haze formations in Guangzhou urban area.

The NO_3 radical formed through the rection between NO_2 and O_3 is the typical nighttime oxidant. Results of Rollins et al. (2012) and Kiendler-Scharr et al. (2016) revealed that NO_3 oxidation of VOCs would contribute substantially to nighttime SOA increase. As shown in Fig.9a, after sunset, the O_3 concentration decreased quickly, however, remained substantially higher than zero, accompanied was the remarkable increases of NO_2 and nitrate. In Guangzhou urban areas, nitrate can either be formed through gas-phase oxidation of NO_2 by OH which forms HNO_3 and then condenses onto aerosol phase, or be formed through the hydrolysis of N_2O_5, which is formed through reactions between NO_2 and NO_3 radical (Yang et al., 2022). The obvious co-increases in nitrate and SOA after sunset indicated that the decrease of O_3 and increase of NO_2 consumption had supplied the NO_3 and N_2O_5 reaction chains and the increase of ALWC favored the hydrolysis of N_2O_5. This was indirectly confirmed when during winter, despite relatively high concentrations of O_3 and NO_2 after sunrise compared with other seasons, nitrate formation was much less prominent due to substantially lower ALWC associated with lower RH. However, the quick increase of SOA still occurred after sunset despite weak daytime SOA formation, suggesting that aqueous reactions might play minor roles in nighttime SOA formation that involve NO_3 radical in Guangzhou urban area. The nighttime chemistry that involves NO_3 radical might contribute substantially to organic nitrate formation (Ng et al., 2008;Fry et al., 2009;Rollins et al., 2012) which would produce the same ions (NO^+ and NO_2^+) with inorganic nitrate due to the fragmentation of nitrate functionality (-ONO2) under 70 eV electron ionization in the aerosol mass spectrometer measurements. However, organic nitrate has different fragmentation pattern with that of inorganic nitrate with previous laboratory studies have shown that the $RN=NO^+/NO_2^+$ of organic nitrate is substantially higher than that of inorganic nitrate. Farmer et al. (2010) thus proposed that the RN variations can be used as an indicator of organic nitrate formations. The Q-ACSM measurements with unit mass resolution cannot provide accurate measurements of RN due to the resolution limitation (Allan et al., 2004), however, the resolved RN related to measured nitrate might provide qualitative constraints on impacts of organic nitrates. The variations of resolved RN as a function of measured nitrate are shown in Fig.10c, which shows that at high levels of nitrate when inorganic nitrate usually

dominates (Xu et al., 2021), the RN approaches near 2.8 which was close to the inorganic nitrate RN reported in (Xu et al., 2021), and locates in the range of 1.1-3.5 of inorganic nitrate RN reported in literatures (Xu et al., 2015). Diurnal variations of RN under different pollution levels shown in Fig.10d reveals higher nighttime RN than daytime, and obvious continuous increase of RN after sunset can be observed for relatively clean and polluted conditions (daily average NR-PM_1 of 20-35 μg/m^3 to NR-PM_1 of 45-60 μg/m^3), suggesting active nighttime organic nitrate formations, which confirmed the involvement of NO_3 radicals in nighttime SOA formations.

4 Implications for future studies

In this study, we highlighted the significant roles of SOA in haze formations in Guangzhou urban area during the entire year and pointed out that for the most prominent and frequent daytime SOA formations all the year around, both gas-phase photochemistry and aqueous reactions played significant roles. Therefore, daytime SOA formation was weak in winter when oxidant level and RH were low, whereas prominent SOA formations were be observed in fall, spring and summer on almost daily basis. However, how gas-phase and aqueous phase reactions have coordinated to promote the SOA formation, and the different contributions of gasSOA and aqSOA to SOA formations under different meteorological conditions and VOCs profiles in different seasons are not clear. In addition, our results suggested that the coordination of daytime and nighttime SOA formation together had resulted in highest SOA concentrations in Guangzhou urban area, thus contributed significantly to severe haze formation. The co-increases of nitrate and SOA after sunrise indicated the significant roles of nighttime NO_3 radical chemistry in promoting haze formations. However, our understanding on how nighttime chemistry evolved and contributed to secondary aerosols formations in different seasons is still highly insufficient in this region. Therefore, the precursors and formation pathways of daytime and nighttime SOA formations and how they coordinated to promote severe haze formations need further comprehensive investigations to make targeted emission control strategies to continuously improve air quality in the PRD region. Also, findings of this study have important implications on future investigations of SOA formation mechanisms in urban areas of southern China that share similar emission sources and meteorological conditions.

Data availability. All data needed are presented in time series of Figures and supplementary Figures, raw datasets of this study are available from the corresponding author Li Liu (liul@gd121.cn) upon request.

Competing interests. The authors declare that they have no conflict of interest.

Author Contributions. YK and LL designed the aerosol experiments. YK conceived and led this research. MMZ and YK wrote the manuscript. MMZ and LL conducted the long-term Q-ACSM measurements. MMZ and YH performed the PMF analysis. HBX, CY, YZ and FL helped maintain and calibrating the Q-ACSM. CL provided meteorological datasets, BL performed the AE33 measurements and post data processing. XJD obtained funding for the continuous aerosol measurements. JCT and WYX provided insights into data analysis, and all authors contributed to revisions of this paper.

Acknowledgments

This work is supported by the Guangdong Provincial Key Research and Development Program (2020B1111360003); National Natural Science Foundation of China (42175083 and 42105092); Guangdong Basic and Applied Basic Research Foundation (2019A1515110791 and 2019A1515011808); National Key Research and Development Program of China (2019YFCO214605); Science and Technology Innovation Team Plan of Guangdong Meteorological Bureau (GRMCTD202003). The Special Fund Project for Science and Technology Innovation Strategy of Guangdong Province（Grant No.2019B121205004.

References

Allan, J. D., Delia, A. E., Coe, H., Bower, K. N., Alfarra, M. R., Jimenez, J. L., Middlebrook, A. M., Drewnick, F., Onasch, T. B., Canagaratna, M. R., Jayne, J. T., and Worsnop, D. R.: A generalised method for the extraction of chemically resolved mass spectra from Aerodyne aerosol mass spectrometer data, Journal of Aerosol Science, 35, 909-922, https://doi.org/10.1016/j.jaerosci.2004.02.007, 2004.

524 Canagaratna, M. R., Jayne, J. T., Jimenez, J. L., Allan, J. D., Alfarra, M. R., Zhang, Q., Onasch, T. B., Drewnick, F., Coe,
525 H., Middlebrook, A., Delia, A., Williams, L. R., Trimborn, A. M., Northway, M. J., DeCarlo, P. F., Kolb, C. E., Davidovits,
526 P., and Worsnop, D. R.: Chemical and microphysical characterization of ambient aerosols with the aerodyne aerosol
527 mass spectrometer, Mass Spectrom Rev, 26, 185-222, 10.1002/mas.20115, 2007.
528 Canonaco, F., Crippa, M., Slowik, J. G., Baltensperger, U., and Prevot, A. S. H.: SoFi, an IGOR-based interface for the
529 efficient use of the generalized multilinear engine (ME-2) for the source apportionment: ME-2 application to
530 aerosol mass spectrometer data, Atmos. Meas. Tech., 6, 3649-3661, 10.5194/amt-6-3649-2013, 2013.
531 Canonaco, F., Tobler, A., Chen, G., Sosedova, Y., Slowik, J. G., Bozzetti, C., Daellenbach, K. R., El Haddad, I., Crippa,
532 M., Huang, R. J., Furger, M., Baltensperger, U., and Prévôt, A. S. H.: A new method for long-term source
533 apportionment with time-dependent factor profiles and uncertainty assessment using SoFi Pro: application to 1
534 year of organic aerosol data, Atmos. Meas. Tech., 14, 923-943, 10.5194/amt-14-923-2021, 2021.
535 Chen, W., Ye, Y., Hu, W., Zhou, H., Pan, T., Wang, Y., Song, W., Song, Q., Ye, C., Wang, C., Wang, B., Huang, S., Yuan,
536 B., Zhu, M., Lian, X., Zhang, G., Bi, X., Jiang, F., Liu, J., Canonaco, F., Prevot, A. S. H., Shao, M., and Wang, X.: Real-
537 Time Characterization of Aerosol Compositions, Sources, and Aging Processes in Guangzhou During PRIDE-GBA
538 2018 Campaign, Journal of Geophysical Research: Atmospheres, 126, e2021JD035114,
539 https://doi.org/10.1029/2021JD035114, 2021a.
540 Chen, W., Ye, Y. Q., Hu, W. W., Zhou, H. S., Pan, T. L., Wang, Y. K., Song, W., Song, Q. C., Ye, C. S., Wang, C. M.,
541 Wang, B. L., Huang, S., Yuan, B., Zhu, M., Lian, X. F., Zhang, G. H., Bi, X. H., Jiang, F., Liu, J. W., Canonaco, F., Prevot,
542 A. S. H., Shao, M., and Wang, X. M.: Real-Time Characterization of Aerosol Compositions, Sources, and Aging
543 Processes in Guangzhou During PRIDE-GBA 2018 Campaign, J Geophys Res-Atmos, 126, ARTN e2021JDO35114
544 10.1029/2021JD035114, 2021b.
545 Drinovec, L., Močnik, G., Zotter, P., Prévôt, A. S. H., Ruckstuhl, C., Coz, E., Rupakheti, M., Sciare, J., Müller, T.,
546 Wiedensohler, A., and Hansen, A. D. A.: The "dual-spot" Aethalometer: an improved measurement of aerosol black
547 carbon with real-time loading compensation, Atmospheric Measurement Techniques, 8, 1965-1979, 10.5194/amt-
548 8-1965-2015, 2015.
549 Ervens, B., Turpin, B. J., and Weber, R. J.: Secondary organic aerosol formation in cloud droplets and aqueous
550 particles (aqSOA): a review of laboratory, field and model studies, Atmos. Chem. Phys., 11, 11069-11102,
551 10.5194/acp-11-11069-2011, 2011.
552 Farmer, D. K., Matsunaga, A., Docherty, K. S., Surratt, J. D., Seinfeld, J. H., Ziemann, P. J., and Jimenez, J. L.: Response
553 of an aerosol mass spectrometer to organonitrates and organosulfates and implications for atmospheric chemistry,
554 Proceedings of the National Academy of Sciences, 107, 6670-6675, doi:10.1073/pnas.0912340107, 2010.
555 Fry, J. L., Kiendler-Scharr, A., Rollins, A. W., Wooldridge, P. J., Brown, S. S., Fuchs, H., Dubé, W., Mensah, A., dal Maso,
556 M., Tillmann, R., Dorn, H. P., Brauers, T., and Cohen, R. C.: Organic nitrate and secondary organic aerosol yield from
557 NO₃ oxidation of β-pinene evaluated using a gas-phase kinetics/aerosol partitioning model, Atmos.
558 Chem. Phys., 9, 1431-1449, 10.5194/acp-9-1431-2009, 2009.
559 Guo, H., Liu, J., Froyd, K. D., Roberts, J. M., Veres, P. R., Hayes, P. L., Jimenez, J. L., Nenes, A., and Weber, R. J.: Fine
560 particle pH and gas–particle phase partitioning of inorganic species in Pasadena, California, during the 2010 CalNex
561 campaign, Atmospheric Chemistry and Physics, 17, 5703-5719, 10.5194/acp-17-5703-2017, 2017.
562 Guo, J. C., Zhou, S. Z., Cai, M. F., Zhao, J., Song, W., Zhao, W. X., Hu, W. W., Sun, Y. L., He, Y., Yang, C. Q., Xu, X. Z.,
563 Zhang, Z. S., Cheng, P., Fan, Q., Hang, J., Fan, S. J., Wang, X. M., and Wang, X. M.: Characterization of submicron
564 particles by time-of-flight aerosol chemical speciation monitor (ToF-ACSM) during wintertime: aerosol
565 composition, sources, and chemical processes in Guangzhou, China, Atmospheric Chemistry and Physics, 20, 7595-
566 7615, 10.5194/acp-20-7595-2020, 2020.
567 He, L. Y., Huang, X. F., Xue, L., Hu, M., Lin, Y., Zheng, J., Zhang, R. Y., and Zhang, Y. H.: Submicron aerosol analysis

568 and organic source apportionment in an urban atmosphere in Pearl River Delta of China using high-resolution
569 aerosol mass spectrometry, J Geophys Res-Atmos, 116, Artn D12304
570 10.1029/2010jd014566, 2011.
571 Huang, X., Ding, A., Gao, J., Zheng, B., Zhou, D., Qi, X., Tang, R., Wang, J., Ren, C., Nie, W., Chi, X., Xu, Z., Chen, L.,
572 Li, Y., Che, F., Pang, N., Wang, H., Tong, D., Qin, W., Cheng, W., Liu, W., Fu, Q., Liu, B., Chai, F., Davis, S. J., Zhang, Q.,
573 and He, K.: Enhanced secondary pollution offset reduction of primary emissions during COVID-19 lockdown in
574 China, National Science Review, 8, nwaa137, 10.1093/nsr/nwaa137, 2021.
575 Huang, X. F., He, L. Y., Hu, M., Canagaratna, M. R., Kroll, J. H., Ng, N. L., Zhang, Y. H., Lin, Y., Xue, L., Sun, T. L., Liu, X.
576 G., Shao, M., Jayne, J. T., and Worsnop, D. R.: Characterization of submicron aerosols at a rural site in Pearl River
577 Delta of China using an Aerodyne High-Resolution Aerosol Mass Spectrometer, Atmospheric Chemistry and Physics,
578 11, 1865-1877, 10.5194/acp-11-1865-2011, 2011.
579 Jayne, J. T., Leard, D. C., Zhang, X. F., Davidovits, P., Smith, K. A., Kolb, C. E., and Worsnop, D. R.: Development of an
580 aerosol mass spectrometer for size and composition analysis of submicron particles, Aerosol Science and
581 Technology, 33, 49-70, Doi 10.1080/027868200410840, 2000.
582 Jimenez, J. L., Jayne, J. T., Shi, Q., Kolb, C. E., Worsnop, D. R., Yourshaw, I., Seinfeld, J. H., Flagan, R. C., Zhang, X. F.,
583 Smith, K. A., Morris, J. W., and Davidovits, P.: Ambient aerosol sampling using the Aerodyne Aerosol Mass
584 Spectrometer, J Geophys Res-Atmos, 108, Artn 8425
585 10.1029/2001jd001213, 2003.
586 Jimenez, J. L., Canagaratna, M. R., Donahue, N. M., Prevot, A. S. H., Zhang, Q., Kroll, J. H., DeCarlo, P. F., Allan, J. D.,
587 Coe, H., Ng, N. L., Aiken, A. C., Docherty, K. S., Ulbrich, I. M., Grieshop, A. P., Robinson, A. L., Duplissy, J., Smith, J. D.,
588 Wilson, K. R., Lanz, V. A., Hueglin, C., Sun, Y. L., Tian, J., Laaksonen, A., Raatikainen, T., Rautiainen, J., Vaattovaara, P.,
589 Ehn, M., Kulmala, M., Tomlinson, J. M., Collins, D. R., Cubison, M. J., Dunlea, J., Huffman, J. A., Onasch, T. B., Alfarra,
590 M. R., Williams, P. I., Bower, K., Kondo, Y., Schneider, J., Drewnick, F., Borrmann, S., Weimer, S., Demerjian, K., Salcedo,
591 D., Cottrell, L., Griffin, R., Takami, A., Miyoshi, T., Hatakeyama, S., Shimono, A., Sun, J. Y., Zhang, Y. M., Dzepina, K.,
592 Kimmel, J. R., Sueper, D., Jayne, J. T., Herndon, S. C., Trimborn, A. M., Williams, L. R., Wood, E. C., Middlebrook, A.
593 M., Kolb, C. E., Baltensperger, U., and Worsnop, D. R.: Evolution of Organic Aerosols in the Atmosphere, Science,
594 326, 1525-1529, 10.1126/science.1180353, 2009.
595 Kiendler-Scharr, A., Mensah, A. A., Friese, E., Topping, D., Nemitz, E., Prevot, A. S. H., Äijälä, M., Allan, J., Canonaco,
596 F., Canagaratna, M., Carbone, S., Crippa, M., Dall Osto, M., Day, D. A., De Carlo, P., Di Marco, C. F., Elbern, H., Eriksson,
597 A., Freney, E., Hao, L., Herrmann, H., Hildebrandt, L., Hillamo, R., Jimenez, J. L., Laaksonen, A., McFiggans, G., Mohr,
598 C., O'Dowd, C., Otjes, R., Ovadnevaite, J., Pandis, S. N., Poulain, L., Schlag, P., Sellegri, K., Swietlicki, E., Tiitta, P.,
599 Vermeulen, A., Wahner, A., Worsnop, D., and Wu, H.-C.: Ubiquity of organic nitrates from nighttime chemistry in
600 the European submicron aerosol, Geophysical Research Letters, 43, 7735-7744, 10.1002/2016gl069239, 2016.
601 Kuang, Y., He, Y., Xu, W., Yuan, B., Zhang, G., Ma, Z., Wu, C., Wang, C., Wang, S., Zhang, S., Tao, J., Ma, N., Su, H.,
602 Cheng, Y., Shao, M., and Sun, Y.: Photochemical Aqueous-Phase Reactions Induce Rapid Daytime Formation of
603 Oxygenated Organic Aerosol on the North China Plain, Environmental science & technology, 54, 3849-3860,
604 10.1021/acs.est.9b06836, 2020.
605 Lei, L., Sun, Y., Ouyang, B., Qiu, Y., Xie, C., Tang, G., Zhou, W., He, Y., Wang, Q., Cheng, X., Fu, P., and Wang, Z.:
606 Vertical Distributions of Primary and Secondary Aerosols in Urban Boundary Layer: Insights into Sources, Chemistry,
607 and Interaction with Meteorology, Environmental science & technology, 55, 4542-4552, 10.1021/acs.est.1c00479,
608 2021.
609 Li, Y. J., Lee, B. P., Su, L., Fung, J. C. H., and Chan, C. K.: Seasonal characteristics of fine particulate matter (PM) based
610 on high-resolution time-of-flight aerosol mass spectrometric (HR-ToF-AMS) measurements at the HKUST
611 Supersite in Hong Kong, Atmos. Chem. Phys., 15, 37-53, 10.5194/acp-15-37-2015, 2015.

Li, Z., Lei, L., Li, Y., Chen, C., Wang, Q., Zhou, W., Sun, J., Xie, C., and Sun, Y.: Aerosol characterization in a city in central China plain and implications for emission control, J Environ Sci (China), 104, 242-252, 10.1016/j.jes.2020.11.015, 2021.

Liu, L., Kuang, Y., Zhai, M., Xue, B., He, Y., Tao, J., Luo, B., Xu, W., Tao, J., Yin, C., Li, F., Xu, H., Deng, T., Deng, X., Tan, H., and Shao, M.: Strong light scattering of highly oxygenated organic aerosols impacts significantly on visibility degradation, Atmos. Chem. Phys., 22, 7713-7726, 10.5194/acp-22-7713-2022, 2022.

Middlebrook, A. M., Bahreini, R., Jimenez, J. L., and Canagaratna, M. R.: Evaluation of Composition-Dependent Collection Efficiencies for the Aerodyne Aerosol Mass Spectrometer using Field Data, Aerosol Science and Technology, 46, 258-271, 10.1080/02786826.2011.620041, 2012.

Mohr, C., DeCarlo, P. F., Heringa, M. F., Chirico, R., Slowik, J. G., Richter, R., Reche, C., Alastuey, A., Querol, X., Seco, R., Penuelas, J., Jimenez, J. L., Crippa, M., Zimmermann, R., Baltensperger, U., and Prevot, A. S. H.: Identification and quantification of organic aerosol from cooking and other sources in Barcelona using aerosol mass spectrometer data, Atmospheric Chemistry and Physics, 12, 1649-1665, 10.5194/acp-12-1649-2012, 2012.

Ng, N. L., Kwan, A. J., Surratt, J. D., Chan, A. W. H., Chhabra, P. S., Sorooshian, A., Pye, H. O. T., Crounse, J. D., Wennberg, P. O., Flagan, R. C., and Seinfeld, J. H.: Secondary organic aerosol (SOA) formation from reaction of isoprene with nitrate radicals (NO₃), Atmos. Chem. Phys., 8, 4117-4140, 10.5194/acp-8-4117-2008, 2008.

Ng, N. L., Herndon, S. C., Trimborn, A., Canagaratna, M. R., Croteau, P. L., Onasch, T. B., Sueper, D., Worsnop, D. R., Zhang, Q., Sun, Y. L., and Jayne, J. T.: An Aerosol Chemical Speciation Monitor (ACSM) for Routine Monitoring of the Composition and Mass Concentrations of Ambient Aerosol, Aerosol Science and Technology, 45, 780-794, Pii 934555189

10.1080/02786826.2011.560211, 2011.

Paatero, P.: The Multilinear Engine—A Table-Driven, Least Squares Program for Solving Multilinear Problems, Including then-Way Parallel Factor Analysis Model, Journal of Computational and Graphical Statistics, 8, 854-888, 10.1080/10618600.1999.10474853, 1999.

Qin, Y. M., Tan, H. B., Li, Y. J., Schurman, M. I., Li, F., Canonaco, F., Prevot, A. S. H., and Chan, C. K.: Impacts of traffic emissions on atmospheric particulate nitrate and organics at a downwind site on the periphery of Guangzhou, China, Atmospheric Chemistry and Physics, 17, 10245-10258, 10.5194/acp-17-10245-2017, 2017.

Rollins, A. W., Browne, E. C., Min, K. E., Pusede, S. E., Wooldridge, P. J., Gentner, D. R., Goldstein, A. H., Liu, S., Day, D. A., Russell, L. M., and Cohen, R. C.: Evidence for NO_x Control over Nighttime SOA Formation, Science, 337, 1210, 10.1126/science.1221520, 2012.

Su, H., Cheng, Y., and Pöschl, U.: New Multiphase Chemical Processes Influencing Atmospheric Aerosols, Air Quality, and Climate in the Anthropocene, Accounts of chemical research, 53, 2034-2043, 10.1021/acs.accounts.0c00246, 2020.

Sun, Y., Du, W., Fu, P., Wang, Q., Li, J., Ge, X., Zhang, Q., Zhu, C., Ren, L., Xu, W., Zhao, J., Han, T., Worsnop, D. R., and Wang, Z.: Primary and secondary aerosols in Beijing in winter: sources, variations and processes, Atmos. Chem. Phys., 16, 8309-8329, 10.5194/acp-16-8309-2016, 2016.

Sun, Y. L., Zhang, Q., Schwab, J. J., Demerjian, K. L., Chen, W. N., Bae, M. S., Hung, H. M., Hogrefe, O., Frank, B., Rattigan, O. V., and Lin, Y. C.: Characterization of the sources and processes of organic and inorganic aerosols in New York city with a high-resolution time-of-flight aerosol mass apectrometer, Atmospheric Chemistry and Physics, 11, 1581-1602, 10.5194/acp-11-1581-2011, 2011.

Sun, Y. L., Wang, Z. F., Dong, H. B., Yang, T., Li, J., Pan, X. L., Chen, P., and Jayne, J. T.: Characterization of summer organic and inorganic aerosols in Beijing, China with an Aerosol Chemical Speciation Monitor, Atmos. Environ., 51, 250-259, 10.1016/j.atmosenv.2012.01.013, 2012.

Sun, Y. L., Wang, Z. F., Fu, P. Q., Yang, T., Jiang, Q., Dong, H. B., Li, J., and Jia, J. J.: Aerosol composition, sources and processes during wintertime in Beijing, China, Atmospheric Chemistry and Physics, 13, 4577-4592, 10.5194/acp-13-4577-2013, 2013.
Sun, Y. L., Wang, Z. F., Du, W., Zhang, Q., Wang, Q. Q., Fu, P. Q., Pan, X. L., Li, J., Jayne, J., and Worsnop, D. R.: Long-term real-time measurements of aerosol particle composition in Beijing, China: seasonal variations, meteorological effects, and source analysis, Atmospheric Chemistry and Physics, 15, 10149-10165, 10.5194/acp-15-10149-2015, 2015.
Sun, Y. L., Xu, W. Q., Zhang, Q., Jiang, Q., Canonaco, F., Preevot, A. S. H., Fu, P. Q., Li, J., Jayne, J., Worsnop, D. R., and Wang, Z. F.: Source apportionment of organic aerosol from 2-year highly time-resolved measurements by an aerosol chemical speciation monitor in Beijing, China, Atmospheric Chemistry and Physics, 18, 8469-8489, 10.5194/acp-18-8469-2018, 2018.
Ulbrich, I. M., Canagaratna, M. R., Zhang, Q., Worsnop, D. R., and Jimenez, J. L.: Interpretation of organic components from Positive Matrix Factorization of aerosol mass spectrometric data, Atmospheric Chemistry and Physics, 9, 2891-2918, 10.5194/acp-9-2891-2009, 2009.
Xu, L., Suresh, S., Guo, H., Weber, R. J., and Ng, N. L.: Aerosol characterization over the southeastern United States using high-resolution aerosol mass spectrometry: spatial and seasonal variation of aerosol composition and sources with a focus on organic nitrates, Atmos. Chem. Phys., 15, 7307-7336, 10.5194/acp-15-7307-2015, 2015.
Xu, W., Kuang, Y., Bian, Y., Liu, L., Li, F., Wang, Y., Xue, B., Luo, B., Huang, S., Yuan, B., Zhao, P., and Shao, M.: Current Challenges in Visibility Improvement in Southern China, Environmental Science & Technology Letters, 7, 395-401, 10.1021/acs.estlett.0c00274, 2020.
Xu, W., Takeuchi, M., Chen, C., Qiu, Y., Xie, C., Xu, W., Ma, N., Worsnop, D. R., Ng, N. L., and Sun, Y.: Estimation of particulate organic nitrates from thermodenuder–aerosol mass spectrometer measurements in the North China Plain, Atmos. Meas. Tech., 14, 3693-3705, 10.5194/amt-14-3693-2021, 2021.
Yang, D., Li, C., Lau, A. K. H., and Li, Y.: Long-term measurement of daytime atmospheric mixing layer height over Hong Kong, Journal of Geophysical Research, 118, 2422-2433, 2013.
Yang, S., Yuan, B., Peng, Y., Huang, S., Chen, W., Hu, W., Pei, C., Zhou, J., Parrish, D. D., Wang, W., He, X., Cheng, C., Li, X. B., Yang, X., Song, Y., Wang, H., Qi, J., Wang, B., Wang, C., Wang, C., Wang, Z., Li, T., Zheng, E., Wang, S., Wu, C., Cai, M., Ye, C., Song, W., Cheng, P., Chen, D., Wang, X., Zhang, Z., Wang, X., Zheng, J., and Shao, M.: The formation and mitigation of nitrate pollution: comparison between urban and suburban environments, Atmos. Chem. Phys., 22, 4539-4556, 10.5194/acp-22-4539-2022, 2022.
Yao, T., Li, Y., Gao, J., Fung, J. C. H., Wang, S., Li, Y., Chan, C. K., and Lau, A. K. H.: Source apportionment of secondary organic aerosols in the Pearl River Delta region: Contribution from the oxidation of semi-volatile and intermediate volatility primary organic aerosols, Atmospheric Environment, 222, 117111, 10.1016/j.atmosenv.2019.117111, 2020.
Yu, Y., Cheng, P., Li, H., Yang, W., Han, B., Song, W., Hu, W., Wang, X., Yuan, B., Shao, M., Huang, Z., Li, Z., Zheng, J., Wang, H., and Yu, X.: Budget of nitrous acid (HONO) at an urban site in the fall season of Guangzhou, China, Atmos. Chem. Phys., 22, 8951-8971, 10.5194/acp-22-8951-2022, 2022.
Zhang, Q., Jimenez, J. L., Canagaratna, M. R., Allan, J. D., Coe, H., Ulbrich, I., Alfarra, M. R., Takami, A., Middlebrook, A. M., Sun, Y. L., Dzepina, K., Dunlea, E., Docherty, K., DeCarlo, P. F., Salcedo, D., Onasch, T., Jayne, J. T., Miyoshi, T., Shimono, A., Hatakeyama, S., Takegawa, N., Kondo, Y., Schneider, J., Drewnick, F., Borrmann, S., Weimer, S., Demerjian, K., Williams, P., Bower, K., Bahreini, R., Cottrell, L., Griffin, R. J., Rautiainen, J., Sun, J. Y., Zhang, Y. M., and Worsnop, D. R.: Ubiquity and dominance of oxygenated species in organic aerosols in anthropogenically-influenced Northern Hemisphere midlatitudes, Geophysical Research Letters, 34, n/a-n/a, 10.1029/2007GL029979, 2007.
Zhang, Q., Jimenez, J. L., Canagaratna, M. R., Ulbrich, I. M., Ng, N. L., Worsnop, D. R., and Sun, Y.: Understanding atmospheric organic aerosols via factor analysis of aerosol mass spectrometry: a review, Analytical and Bioanalytical

Chemistry, 401, 3045-3067, 10.1007/s00216-011-5355-y, 2011.
Zhang, Y. J., Tang, L. L., Wang, Z., Yu, H. X., Sun, Y. L., Liu, D., Qin, W., Canonaco, F., Prevot, A. S. H., Zhang, H. L., and Zhou, H. C.: Insights into characteristics, sources, and evolution of submicron aerosols during harvest seasons in the Yangtze River delta region, China, Atmospheric Chemistry and Physics, 15, 1331-1349, 10.5194/acp-15-1331-2015, 2015.
Zhao, J., Qiu, Y., Zhou, W., Xu, W., Wang, J., Zhang, Y., Li, L., Xie, C., Wang, Q., Du, W., Worsnop, D. R., Canagaratna, M. R., Zhou, L., Ge, X., Fu, P., Li, J., Wang, Z., Donahue, N. M., and Sun, Y.: Organic Aerosol Processing During Winter Severe Haze Episodes in Beijing, Journal of Geophysical Research: Atmospheres, 124, 10248-10263, 10.1029/2019JD030832, 2019.
Zhou, W., Xu, W., Kim, H., Zhang, Q., Fu, P., Worsnop, D. R., and Sun, Y.: A review of aerosol chemistry in Asia: insights from aerosol mass spectrometer measurements, Environmental Science: Processes & Impacts, 22, 1616-1653, 10.1039/D0EM00212G, 2020.